IEEE Access
Multidisciplinary | Rapid Review | Open Access Journal

Received August 2, 2018, accepted September 2, 2018, date of publication September 5, 2018,
date of current version September 28, 2018.

Digital Object Identifier 10.1109/ACCESS.2018.2868817

A Dual-Broadband Dual-Polarized Fylfot-Shaped Antenna for Mobile Base Stations Using MIMO Over-Lapped Antenna Subarrays

AHMED ALIELDIN[1], YI HUANG[1], (Senior Member, IEEE), STEPHEN J. BOYES[2], (Member, IEEE), MANOJ STANLEY[1], SUMIN DAVID JOSEPH[1], AND BAHAA AL-JUBOORI[1]

[1]Department of Electrical Engineering and Electronics, University of Liverpool, Liverpool L69 3GJ, U.K.
[2]Defence Science and Technology Laboratory, Salisbury SP4 0JQ, U.K.

Corresponding author: Yi Huang (yi.huang@liverpool.ac.uk)

This work was supported by the University of Liverpool.

ABSTRACT This paper proposes a novel design of a dual-broadband dual-polarized antenna for mobile communication base stations. The proposed antenna is Fylfot-shaped and covers 0.7–0.96 and 1.7–2.7 GHz simultaneously (with S11 ≤ -10 dB), which are the two common frequency bands for mobile communication systems. Three resonant frequencies are produced in the proposed design where two of them are independently controlled to achieve the dual-broadband performance. A prototype of the proposed antenna has been developed and tested. The results demonstrate that the antenna has high isolation between its ports, high polarization purity, and stable radiation patterns across both the frequency bands. A new linear array is proposed and implemented. Unlike reported dual-band base station antenna arrays, the proposed array uses a novel technique of two MIMO overlapped subarrays with shared radiating antenna elements. The overlapped subarrays have excellent frequency diversity performance with low envelope correlation coefficients. The array has been found to have the same performance as a standard conventional base station antenna but with 25% less number of antenna elements, which leads to a smaller size and lower cost. The simple antenna structure and the novel smart MIMO overlapped antenna subarrays technique give the design the privilege to be an ideal candidate for a low-cost directive base station antenna.

INDEX TERMS Antenna array, base station, dual-broadband, dual-polarized, Fylfot-shaped, over-lapped.

I. INTRODUCTION

The evolution of smartphone technology has resulted in the development of base station antennas for mobile communication systems from single-polarized to dual-polarized and from single band to dual or multi-bands [1]. The most common frequency bands used for mobile communication systems are the lower band (LB) from about 0.7 to 0.96 GHz and the upper band (UB) from 1.7 to 2.7 GHz. To increase the data rate and channel capacity and reduce the signal fading in a multipath environment, space diversity and/or polarization diversity are commonly used [2]. Base station antenna designers face many challenges such as to obtain a stable radiation pattern within the desired frequency bands, high polarization purity (PP) and good impedance matching at the same time [3]. The PP is defined as the ratio of co- and cross-polarization in two orthogonal planes (typically $\pm 45°$ for base station antennas). It is favourable to have a low-cost design with a small size and low profile as well. Many successful designs have been introduced in the literature to meet these specifications for a single band antenna (either the LB or the UB) using planar cross dipoles [4] or 3D-printed dipoles [5], [6].

The most challenging task is to get a compact design which covers dual or multi-bands. There are quite a few published designs. A dual-broadband antenna was reported in [7] but its single polarization characteristic limits its use as a base station antenna. In [8], a dual-polarized dual-band antenna array was designed using two different collocated elements to cover the two bands, an arc-probe-fed ring antenna for the LB and a printed microstrip dipole antenna for the UB. Moreover, in [9]–[11], two 3D pairs of cross-dipoles are used to widen the bandwidth (BW) (one pair for each band). Again they are collocated to reduce the antenna size. Later on, multi-band arrays have been achieved using three or more different

frequency band elements with embedded scheme [12] or optimal array structure [13]. For more size reduction in dual-band base station antenna arrays, the UB elements are embedded inside the 3D octagonal-shaped LB elements which are formed as bowls [14]. Although a high isolation between the two collocated elements is achieved, the BW is insufficient to cover the whole LB and UB. In [15], the BW has been improved using a similar embedded array structure as in [14] but the radiation pattern half power beam width (HPBW) at the UB is 90° which is not suitable to be employed in densely populated urban areas (typically 65 ± 5°) [16] in addition to the antenna large size.

Generally, most of the designs presented in the literature use different element designs for different frequency bands. In [17]–[20], the approach of covering both bands (the LB and UB) by a single antenna element was adopted but with some limitations in the BWs which were insufficient to cover all the desired frequencies. Also, the large antennas size obligates the spacing between the elements to be larger than one wavelength when they are arranged to form linear UB antenna arrays. Thus, undesirable grating lobes may be formed. Moreover, some of these dual-band elements have complicated multilayer structures [17], [18] while others provide a single polarization [19], [20].

In this paper, a novel Fylfot-shaped antenna design is introduced to cover both the LB and the UB simultaneously with a dual-polarization. The antenna enjoys good impedance matching and high PP with a low cost and a compact size. The design is extended to form a linear antenna array using a novel Multiple Input Multiple Output (MIMO) over-lapped antenna subarray (OLAS) technique. Although two subarrays are over-lapped and share some radiating antenna elements, they have an excellent frequency diversity performance with low Envelope Correlation Coefficients (ECC).

The paper is organized as follows: Section II describes the dual-band antenna design, its principle of operations, initial results and its performance. Section III presents the development of MIMO OLAS base station. Finally, conclusions are drawn in Section IV.

II. FYLFOT-SHAPED ANTENNA ELEMENT

A. ANTENNA STRUCTURE

Fig. 1 presents the proposed antenna element geometry while Table 1 illustrates its dimensional parameters. Generally, the antenna element can be described as two orthogonal slotted elliptical-shaped cross dipoles printed on opposite sides of an FR-4 substrate with relative permittivity $\varepsilon_r = 4.3$, tangential loss of 0.025, thickness Hd = 1.6 mm and side length Ld. The dipoles are placed on ±45° with respect to Y-axis in order to provide polarization diversity. Each dipole consists of two elliptical-shaped elements linked by a feeding strip and an RF connector.

The endpoints of each slotted elliptical-shaped dipole are extended to form a bowtie dipole which is placed orthogonal to the ellipse major axis forming a Fylfot shape. Thus, again the bowtie dipoles on both sides of the substrate are placed

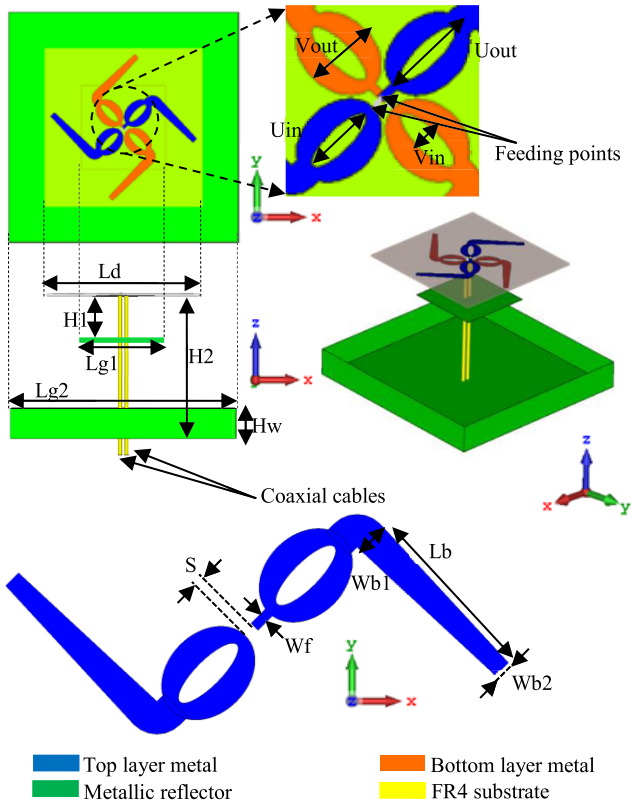

FIGURE 1. The geometry of the proposed antenna element.

TABLE 1. Parameters of the proposed antenna.

Parameter	Value (mm)
Vout	22
Uout	29
Vin	7
Uin	19
Lb	52
Wb1	9
Wb2	5
Wf	3
S	4
Ld	150
Lg1	80
Lg2	220
H1	30
H2	100
Hw	23

on ±45° with respect to Y-axis. The substrate and dipoles are oriented in the XY plane. The substrate is placed above two square metallic ground reflectors to enable directional radiation; a small reflector and a large reflector are used for the UB and LB beam radiation respectively. The small reflector is placed at a height H1 and has a side length Lg1 while the large reflector is placed at a height H2, with side length Lg2 and four sidewalls of a height Hw. The four sidewalls work as four parasitic elements allocated at ± 45° with respect to the radiating dipoles to improve the PP [4]. The substrate and the two metallic reflectors are concentric, and their edges are parallel to X and Y-axes. The antenna is

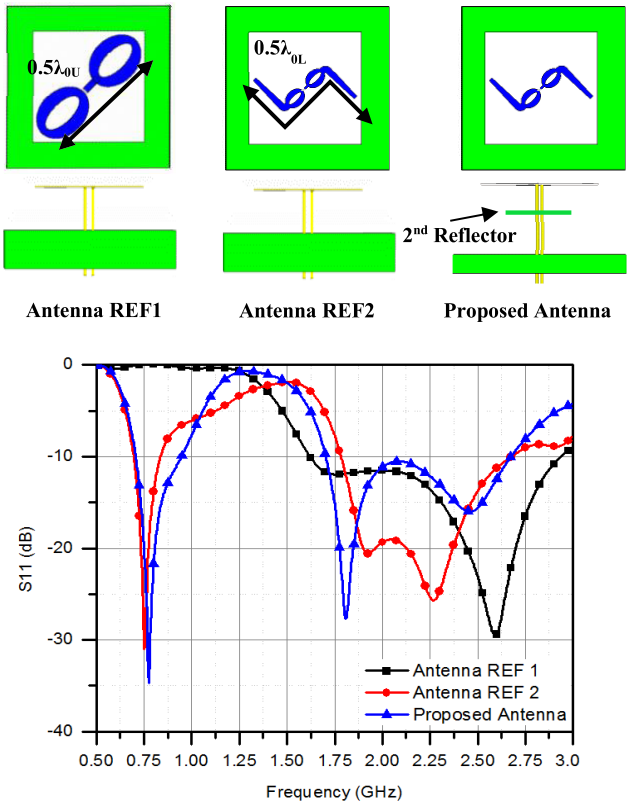

FIGURE 2. References and the proposed antennas.

fed through two coaxial cables. The outer of the coaxial cable is connected to one of the elliptical elements of the antenna while the inner is connected to the strip line.

B. ANTENNA PRINCIPLES OF OPERATION

The proposed antenna can be considered as two different types of dipoles printed on each side of the substrate and connected together, a slotted elliptical-shaped dipole and a bowtie dipole. To understand the working principle of the proposed antenna, two reference designs (antenna REF1 and antenna REF2) are used as shown in Fig. 2. Initially, the design was based on the UB antenna, which has been presented and illustrated by the authors in [21] (antenna REF1). The slotted elliptical-shaped dipole length (2Uout) equals to $0.5\lambda_{0U}$ (where λ_{0U} is the free space wavelength of the central frequency at the UB 2.2 GHz). It is observed that antenna REF1 has two resonant frequencies at the UB, one is due to the long current path from the feeding points to the ellipse endpoints along the ellipse edges and the other is due to the short current path from the feeding points to the ellipse endpoints along the elliptical slot edges. Antenna REF1 covers the UB only as shown in Fig. 2.

The design is amended by adding a bowtie dipole with a length of (2Lb) to the slotted elliptical-shaped dipole. Each pole of the bowtie dipole is connected to one of the endpoints of the slotted elliptical-shaped dipole and forming 90° with respect to the ellipse major axis (antenna REF2). Thus, the bowtie dipoles on both sides are orthogonal and placed

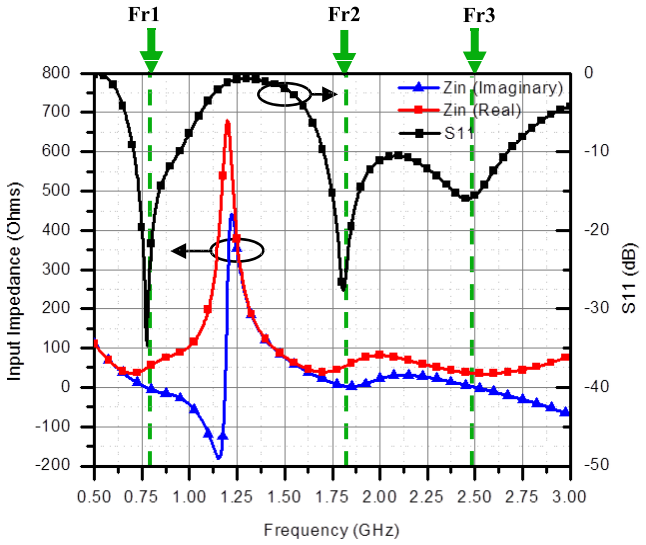

FIGURE 3. Input impedance of the proposed antenna correlated to S11.

on ±45° with respect to Y-axis. The dimension Lb was initially selected such that the dipoles total length (2Uout+2Lb) equals to $0.5\lambda_{0L}$ (where λ_{0L} is the free space wavelength of the central frequency at the LB 0.83 GHz). It is evident that a third resonant frequency has been created at the LB as shown in Fig. 2 but unfortunately, the BW at the UB has been shrunk.

A second small metallic reflector is placed at a height H1 with respect to the substrate (proposed antenna).This second reflector has two functions; the first one is to improve the impedance matching across the UB as will be discussed in detail in section II.D. The second function is to enable directional radiation for the signal in the UB. The dimensions H1 and H2 were initially selected to be $0.25\lambda_{0U}$ and $0.25\ \lambda_{0L}$ respectively.

The input impedance (Zin) of the proposed antenna in correlation to the reflection coefficient is presented in Fig. 3. The three resonant frequencies (Fr1 at the LB and Fr2, Fr3 at the UB) are located at the points where the imaginary part of Zin (Im (Zin)) equals to zero. Fr1, Fr2 and, Fr3 are 0.77, 1.84 and 2.5 GHz respectively. One of the advantages of this design is that Fr1 and Fr3 can be controlled independently of one another and of Fr2, as going to be discussed in detail in section II.C. So, once Fr2 is obtained, Fr1 and Fr3 can be independently tuned and dual-broadband can be achieved. Note that the values of the real part of Zin (Re (Zin)) around these resonant frequencies satisfy VSWR ≤ 2 ($Z_0/2 \leq$ Re (Zin) $\leq 2Z_0$) where Z_0 is the characteristic impedance (50Ω in our case).

The current distributions across the radiating dipoles at the three resonant frequencies are shown in Fig. 4. It can be seen that at Fr1, the current flows from the feeding point to the terminal points through both dipoles (slotted elliptical-shaped and bowtie dipoles) uniformly. This means that both dipoles contribute in forming impedance matching at the LB. On the other hand, the current distributions at Fr2 and Fr3 is highly dense around the slotted elliptical-shaped dipole while

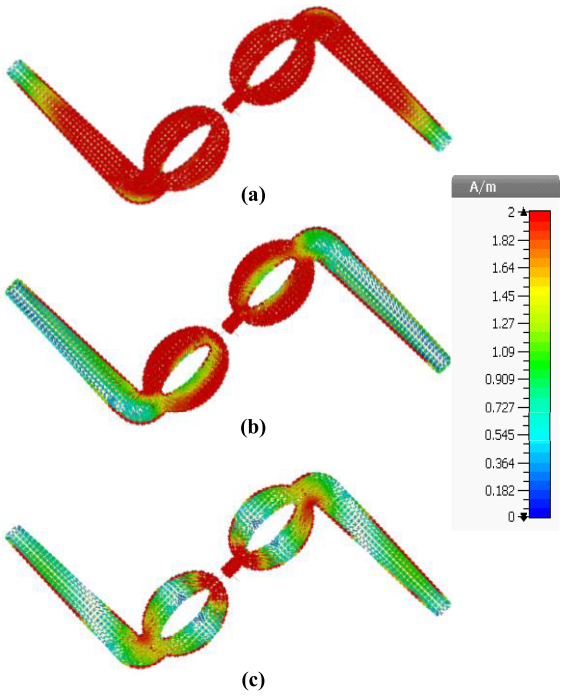

FIGURE 4. The current distributions at (a) Fr1 (b) Fr2 (c) Fr3.

there is a light current density across the bowtie dipole. So, we can conclude that the elliptical-shaped dipole contributes in creating impedance matching across both bands while bowtie dipole mainly affects the LB only.

By adjusting the dimensions of the feeding lines, the elliptical-shaped dipoles, the elliptical slot, and the bowtie dipoles, it is possible to achieve good impedance matching. By appropriately designing the reflectors and adjusting their height from the substrate, a stable radiation pattern with high gain and suitable half power beam width (HPBW) for base station antenna can be achieved.

To validate the proposed design, a prototype was fabricated and tested as shown in Fig. 5. The PCB and the small reflector are fixed above the large reflector using foam layers. It is favourable to use pillars to fix the antenna pieces altogether to make it more rigid mechanically in case of industrial usage.

Fig. 6 shows a good agreement between the simulated and measured reflection coefficients. For S11 ≤ -10 dB, the measured fractional BWs are 40% (0.7-1.05 GHz) and 60% (1.6 -3 GHz) for the LB and UB respectively. Fig. 7 shows that the measured port-to-port isolation is better than 30 dB for the LB and better than 20 dB for the UB. The isolation at the UB is less than the isolation at the LB because of the high surface current density for the UB formed at the feed point of the antenna (see Fig. 4), which can couple to the other orthogonal dipole. The deviation between the simulated and the measured port-to-port isolations may be due to fabrication tolerance.

The simulated and measured co- and cross-polarized radiation patterns at the start, central and end frequencies of each band in H-plane (XZ plane) and V-plane (YZ plane) are

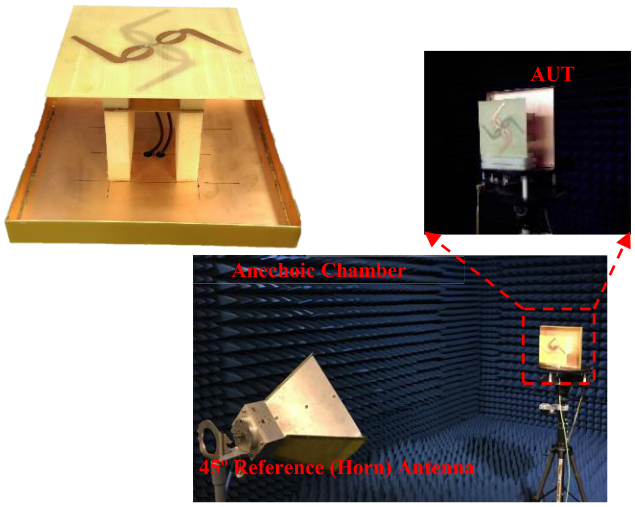

FIGURE 5. A prototype of the proposed antenna element.

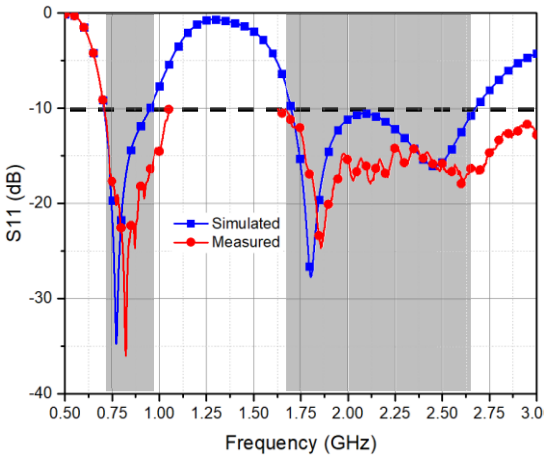

FIGURE 6. Simulated and measured reflection coefficients.

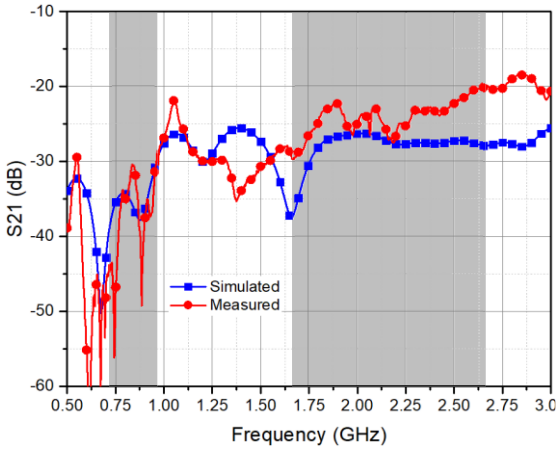

FIGURE 7. Simulated and measured port-to-port isolation.

shown in Fig. 8. It is apparent that the proposed antenna has a good agreement in radiation pattern between the simulation and the measurement results. The HPBWs in the H-plane are

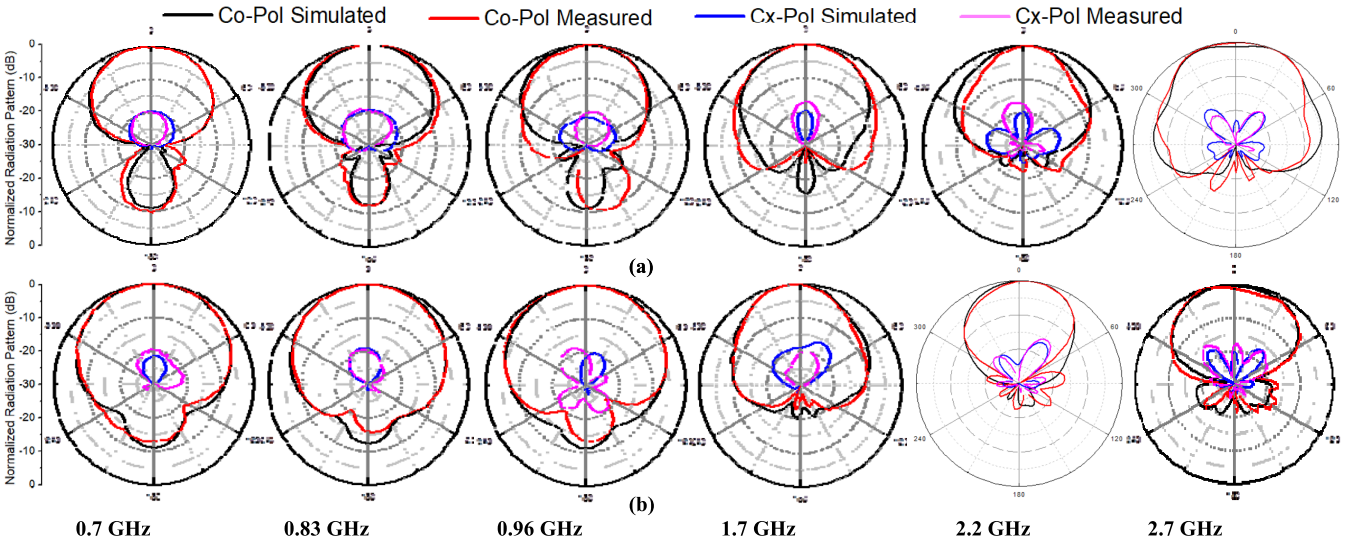

FIGURE 8. Simulated and measured co- and cross-polarized radiation patterns in (a) H-plane (b) V-plane.

TABLE 2. PP at boresight of the proposed antenna.

Frequency Band	Frequency (GHz)	PP (dB)
LB	0.7	20.8
	0.83	20.5
	0.96	20.3
UB	1.7	18
	2.2	19.6
	2.7	18.3

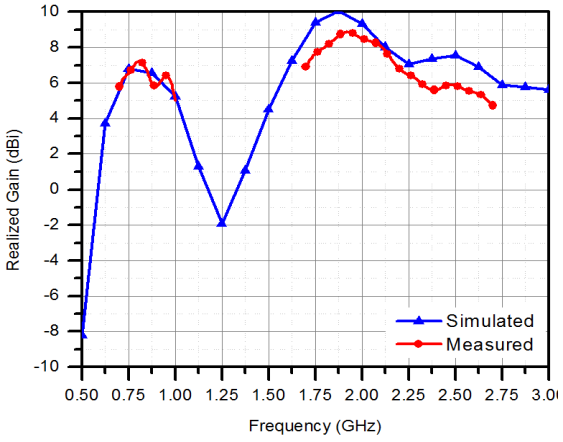

FIGURE 9. Simulated and measured realized gain of the proposed antenna.

73±2° and 65±5° at the LB and UB while the HPBWs in the V-plane are 90±5° and 72±8° at the LB and the UB respectively. PP at boresight is better than 20 dB at the LB and better than 18 dB for the UB. The detailed values of PP are illustrated in Table 2.

Fig. 9 presents the simulated and measured realized gains of the proposed antenna at the LB and UB. The realized gain is 6±1 dBi and 6.7±2 dBi at the LB and UB respectively.

Table 3 displays a comparison between the state-of-the-art dual-band dual-polarized base station antenna elements performance and the proposed antenna. It is apparent that the proposed antenna is an optimum design which has a relatively wide BW, suitable HPBWs for base station antennas employed in densely populated urban areas and, a small size. Also, it has a simple manufacturing process using PCB instead of the 3D printing used in [10], [11], [14], and [15]. The most important feature in the proposed antenna is that it covers both bands simultaneously which gives it the privilege to be used as a shared element between the LB and the UB subarrays at the same time in a base station antenna as will be discussed in detail in section III.

To optimize the proposed antenna design, it is necessary to understand how the design parameters affect the antenna performance. So, some important parameters and their effects are studied through simulations. When one parameter is studied, all other parameters are kept constant.

C. EFFECT OF DIPOLES DIMENSIONS

Controlling the two resonant frequencies (Fr1 and Fr3) independently is the key-point of achieving dual-broadband. Therefore, in this section, we are going to present these controlling dimensional parameters.

The first parameter to be studied is the bowtie dipole length (Lb). As the antenna working principles have been discussed in section II.B, the bowtie dipoles contribute in the impedance matching across the LB only with a very slight effect on the UB. Thus, Fr1 can be controlled independently of Fr2 and Fr3 by changing the length Lb. As noticed in Fig. 10, when the length Lb increases, the overall length of the dipole (2Lb+2Uout) increases while the length of the elliptical dipole (2Uout) remains constant. Thus the LB is shifted to lower frequencies while the UB has almost no changes. The optimum value of Lb is found to be 52 mm to cover the whole LB with VSWR $\leq$ 2.

TABLE 3. Comparison of several dual-band dual-polarized antennas.

Ref		[10]	[11]	[14]	[15]	[19]	Proposed Antenna
Frequency Band(GHz)	LB	0.79 - 1	0.79 – 0.96	0.79 – 0.96	0.7 – 1.18	0.78 – 1.02	**0.7 – 1.05**
	UB	1.64 – 2.76	1.71 – 2.17	1.71 – 2.17	1.67 – 2.73	2.04 – 3.13	**1.6 - 3**
BW (%)	LB	23.5 (VSWR ≤ 2)	19.4 (VSWR ≤ 1.5)	19.4 (VSWR ≤ 1.5)	51 (VSWR ≤ 1.5)	26.6 (VSWR ≤ 2)	**40 (VSWR ≤ 2)**
	UB	51 (VSWR ≤ 2)	23.7 (VSWR ≤ 1.5)	23.7 (VSWR ≤ 1.5)	48 (VSWR ≤ 1.5)	42.2 (VSWR ≤ 2)	**60 (VSWR ≤ 2)**
HPBW(°)	LB	69	64.5	65	61.5	60	**73**
	UB	73	66	65	90	50	**65**
Gain (dBi)	LB	8.6	9.3	9.5	8.4	8.4	**6**
	UB	8.8	9	9	8.7	8	**6.7**
Size (mm^3)	Without reflectors	135×135×75	152×152×71	166×166×68	152×152×100	125×125×16	**150×150×1.6**
	With reflectors	140×140×75	255×255×71	255×255×130	290×290×100	244×244×50	**220×220×100**
Manufacturing Process		3D printing	3D printing	3D printing	3D printing	PCB	**PCB**
Number of Elements		1 for the LB + 1 for the UB	1 for the LB + 1 for the UB	1 for the LB + 2 for the UB	1 for the LB + 1 for the UB	1 for the LB + 1 for the UB	**1 for both bands**

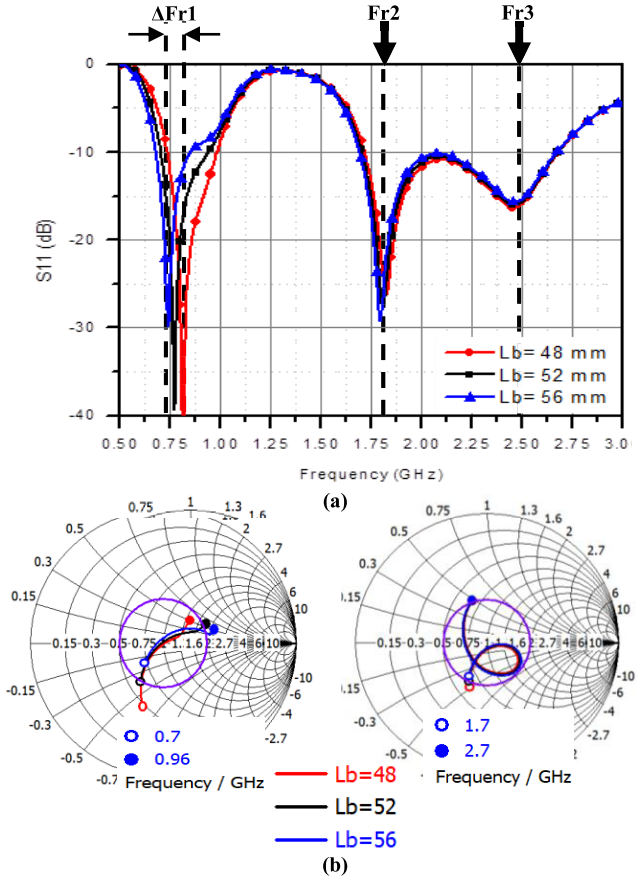

FIGURE 10. The effect of Lb on the impedance matching illustrated by (a) reflection coefficient (b) Smith charts.

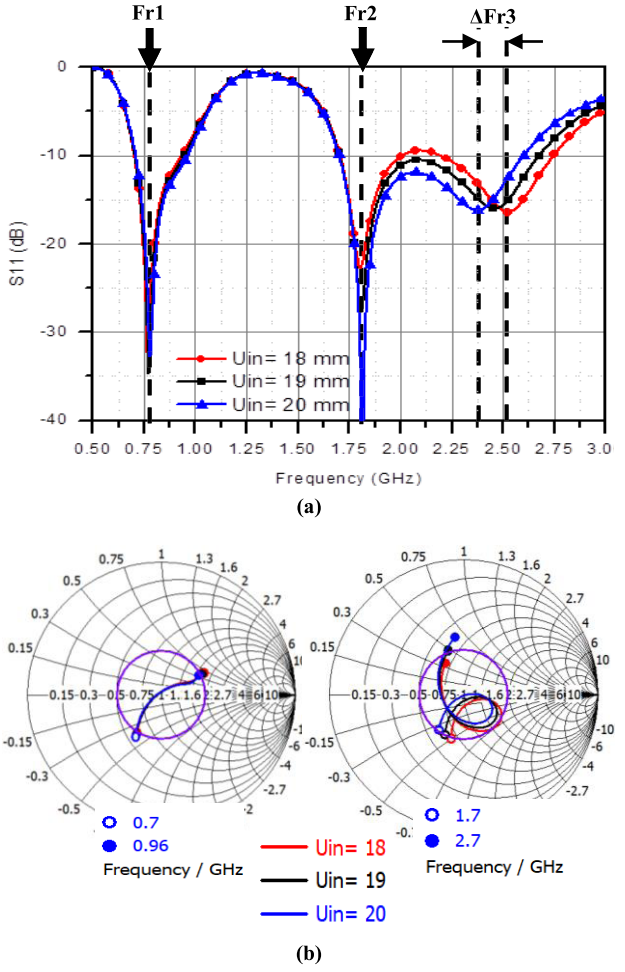

FIGURE 11. The effect of Uin on the impedance matching illustrated by (a) reflection coefficient (b) Smith charts.

The second parameter to be studied is the elliptical-slot major axis Uin. Changing Uin does not result in any changes in the two dipoles length. Thus, it has almost no effect on the first and the second resonant frequency (Fr1 and Fr2). The third resonant frequency Fr3 can be tuned by changing the dimension Uin as shown in Fig. 11. The optimum value of Uin is found to be 19 mm to fully cover the UB.

D. EFFECT OF THE SMALL METALLIC REFLECTOR

The small reflector has two functions in the antenna performance enhancement.

The first function is improving the antenna BW at the UB. Although there are two independent resonant frequencies at

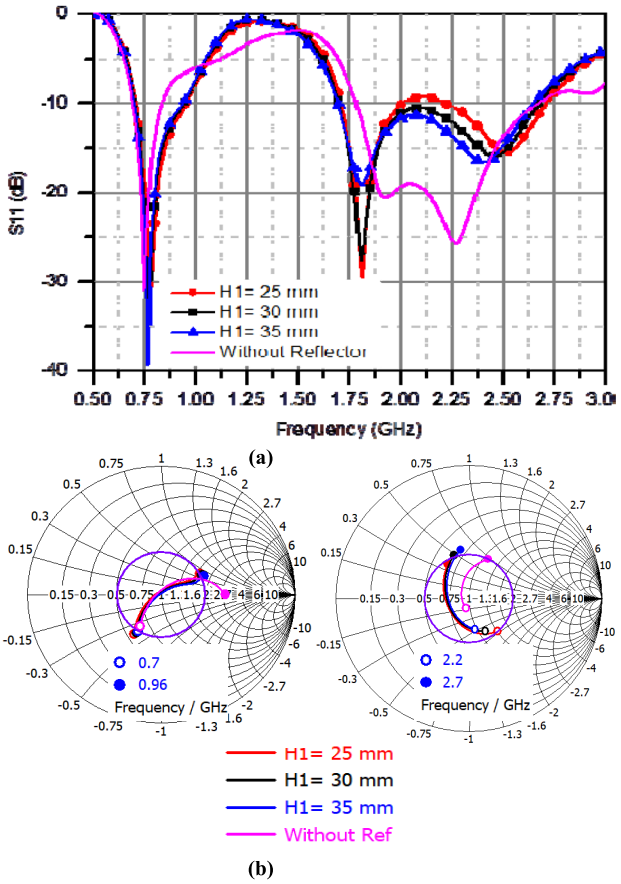

FIGURE 12. The effect of the small reflector on the impedance matching illustrated by (a) reflection coefficient (b) Smith charts.

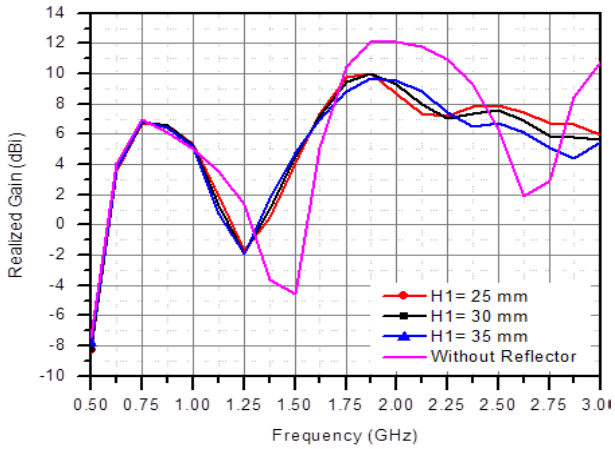

FIGURE 13. The effect of the small reflector on the realized gain.

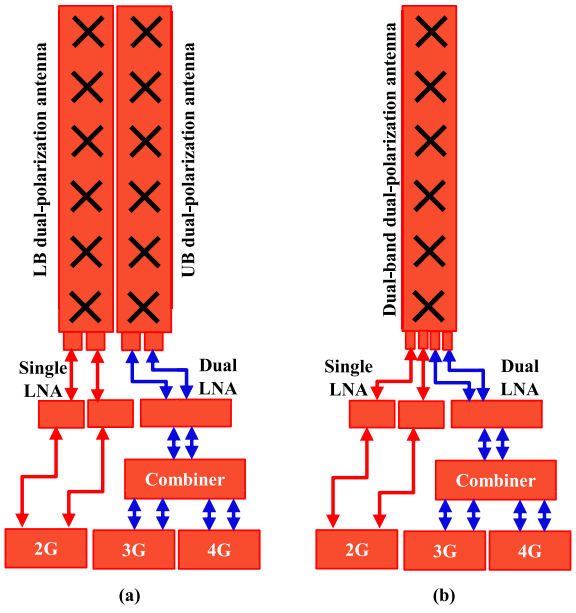

FIGURE 14. Illustrative diagrams of the (a) conventional (b) proposed MIMO OLAS base station.

the UB, it is not possible to achieve full coverage across the whole UB without the small reflector as shown in Fig. 12. From Fig. 12(a), the height H1 affects only Fr3 with almost no effect on Fr1 and Fr2. By investigating the effect of changing H1 on the dipole input impedance around Fr3 (2.2-2.7 GHz), we notice from the Smith chart in Fig. 12(b) that the small reflector adds a capacitive loading to the radiating dipoles at Fr3. Thus, when the height H1 increases, the capacitive loading decreases and the plot goes inductive at Fr3. The optimum height H1 is 30 mm to get the best achievable impedance matching. Note that there is almost no significant change in the impedance matching across the LB.

The second function is improving the antenna gain stability of the UB radiated signal as it enables the unidirectional radiation by reflecting most of the back radiation at this band as illustrated in Fig. 13. It is noticeable that the small reflector has no effect on the antenna gain at the LB.

III. MIMO OVER-LAPPED ANTENNA SUBARRAYS

Directive base station antennas are formed in linear arrays with high gains typically 12-14 and 15-17 dBi for the LB and UB antenna arrays respectively [22]. The conventional base station antenna array diagram is presented in Fig. 14(a). It consists of two linear arrays, typically one array for each band. These arrays may be totally disjointed but mostly they are collocated in the same radome to reduce the antenna size. However, in all cases, each array uses its own antenna element structure and a separate feeding network. In this section, a proposed single linear array is constructed using two MIMO OLAS, a sub-array for each band. Unlike the base station arrays reported in the literature, these two MIMO OLAS shared some of their radiating elements (i.e. some antenna elements contribute in forming the radiation patterns of both sub-arrays simultaneously). So, the proposed antenna array can take the role of both the LB and UB arrays in the conventional base station antenna with fewer elements as shown in Fig. 14(b). The proposed array consists of two sub-arrays: the LB subarray and the UB subarray. Thus, the sub-arrays have frequency diversity. The number of elements N in

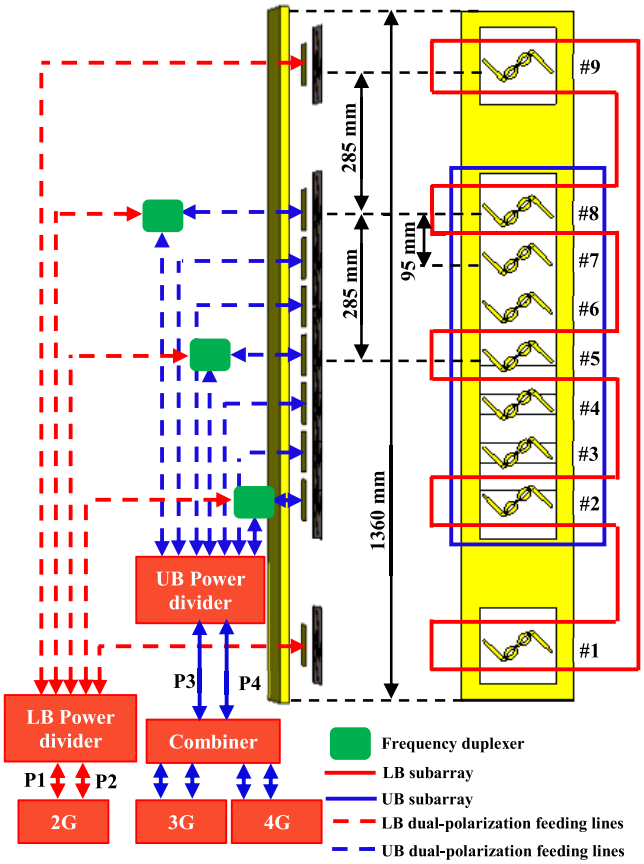

FIGURE 15. The proposed 9-element MIMO OLAS base station.

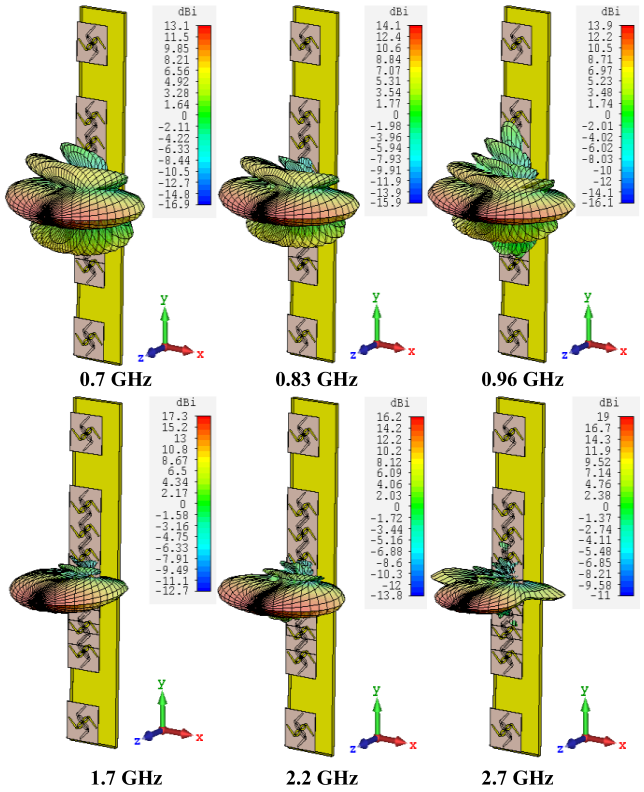

FIGURE 16. Simulated 3D radiation patterns of the OLAS base station.

each subarray may be found by [23]:

$$N = \frac{D\lambda_0}{2d} \tag{1}$$

where D is the subarray directivity and d is the distance between two successive elements in the subarray. To avoid high coupling between elements and grating lobes, d is selected as $0.5\lambda_{max} < d < \lambda_{min}$ [23] where λ_{max} is the free space wavelength at the start frequency of the desired band (0.7 GHz for the LB and 1.7 GHz for the UB) and λ_{min} is the free space wavelength for the end frequency of the desired band (0.96 GHz for the LB and 2.7 GHz for the UB). So, d is chosen to be 285 mm for the LB subarray and 95 mm for the UB subarray.

Note that for practical implementation, d in the LB subarray is three times d in the UB subarray. From equation (1), the number of elements in each subarray is five and seven elements for the LB and UB subarrays respectively.

To build such subarrays, a 9-element antenna array is constructed with elements distributed as shown in Fig. 15. The UB subarray consists of the middle elements numbering from 2 to 8 with a total number of seven elements while the LB subarray consists of five elements numbered 1, 2, 5, 8, and 9. Note that element number 2, 5 and 8 are shared between the two subarrays. So, virtually, the total number of elements in both subarrays are twelve (five elements for the LB subarray and seven elements for the UB subarray) while the actual number of elements is nine. This means a 25% reduction in elements capacity which leads to a reduction in antenna size and cost. Each one of the shared antenna elements numbered 2, 5 and 8 is fed through a frequency duplexer. The input port of the frequency duplexer is connected to the antenna element while its output ports are connected to the LB and UB power dividers respectively. In the receiving mode, the LB and UB signals propagate from the antenna to the input port of the duplexer which in turns directs each signal to the corresponding output port and hence to the corresponding power divider. In the transmitting mode, this process is reversed. Each subarray is fed through two ports for two orthogonal polarizations (P1 and P2 for $\pm 45°$ of the LB subarray and P3 and P4 for $\pm 45°$ of the UB subarray respectively). The Feeding network including the power dividers, the frequency duplexers and feeding ports is presented in Fig. 15.

Two different types of diversity are used in the proposed MIMO OLAS to enhance the communication performance: polarization diversity between the dipoles in each antenna element and frequency diversity between the subarrays. The overall array height is 1360 mm which is smaller than the conventional base station antenna array height (typically 1500 mm) [22].

Fig. 16 shows the simulated 3D radiation patterns and gains of the proposed antenna array at each band. It is seen that the gains are 13.5 and 17.6 dBi at the LB and UB respectively.

TABLE 4. Comparison of standard and several dual-band base station antenna arrays.

Ref		Standard base station antenna [22]	[14]	Proposed Antenna
Total Number of Elements		The fewer, the better	15	**9**
Number of Element Types		The fewer, the better	3	**1**
Overall Size (mm^3)		The smaller, the better	1420×260×130	**1360×220×100**
Realized Gain (dBi)	LB	12-14	15	**13.5**
	UB	15-17	17.3	**17.6**
FBR (dB)	LB	≤ 25	25	**27**
	UB	≤ 25	25	**29**

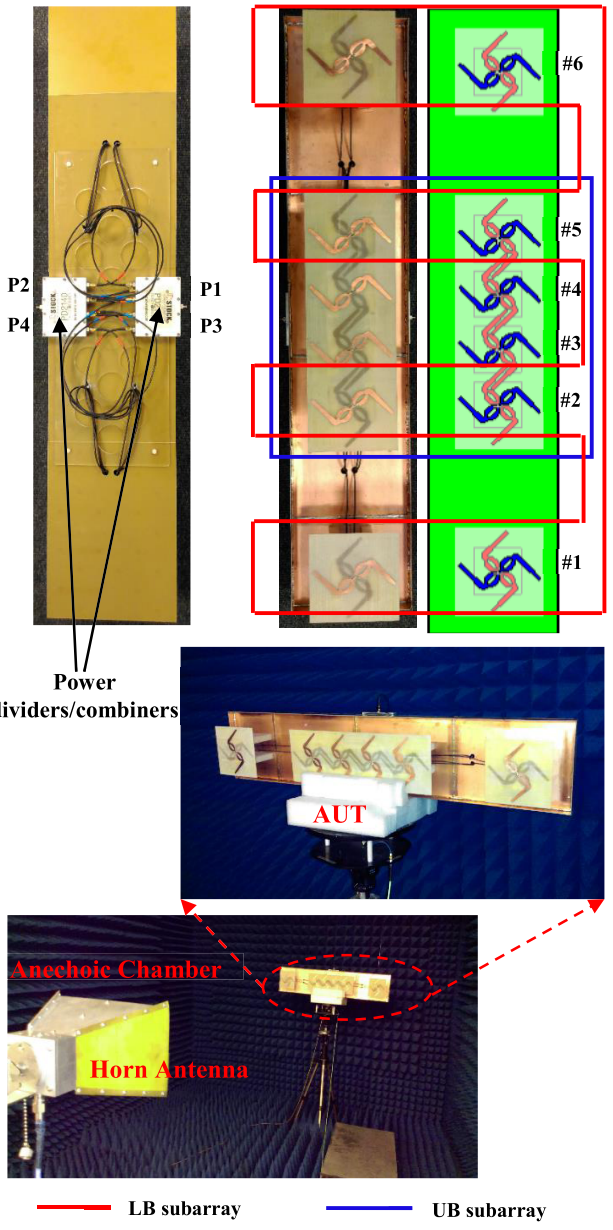

FIGURE 17. A Prototype of the proposed MIMO OLAS base station.

The proposed MIMO OLAS is compared to the standard base station antenna and the state-of-the-art array presented in [14] and the comparison is tabulated in Table 4. From the

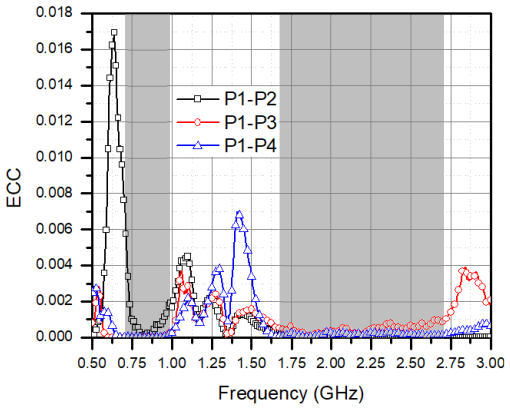

FIGURE 18. Measured ECC of the ports of the proposed MIMO OLAS.

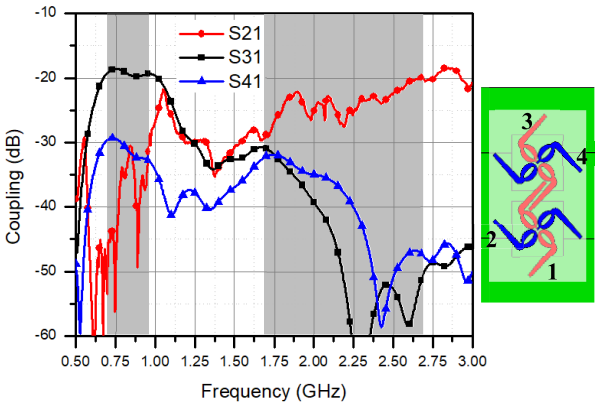

FIGURE 19. Measured isolation between two adjacent elements in the proposed MIMO OLAS.

comparison, we notice that although the electrical specifications (front-to-back lobe ratios (FBR) and realized gains) for both arrays are comparable to each other and meet the specifications of the standard base station antenna, the proposed antenna array has remarkable better mechanical specifications (a fewer number of elements, a smaller size and, a simpler manufacturing technique). Also, the array in [14] uses three different types of elements to cover the LB and UB (one for the LB and two for the UB) while the proposed array uses the same antenna element for both bands.

To validate the MIMO OLAS design, a small-scale prototype was fabricated. The prototype array has two subarrays each one contains four elements. So, virtually the total

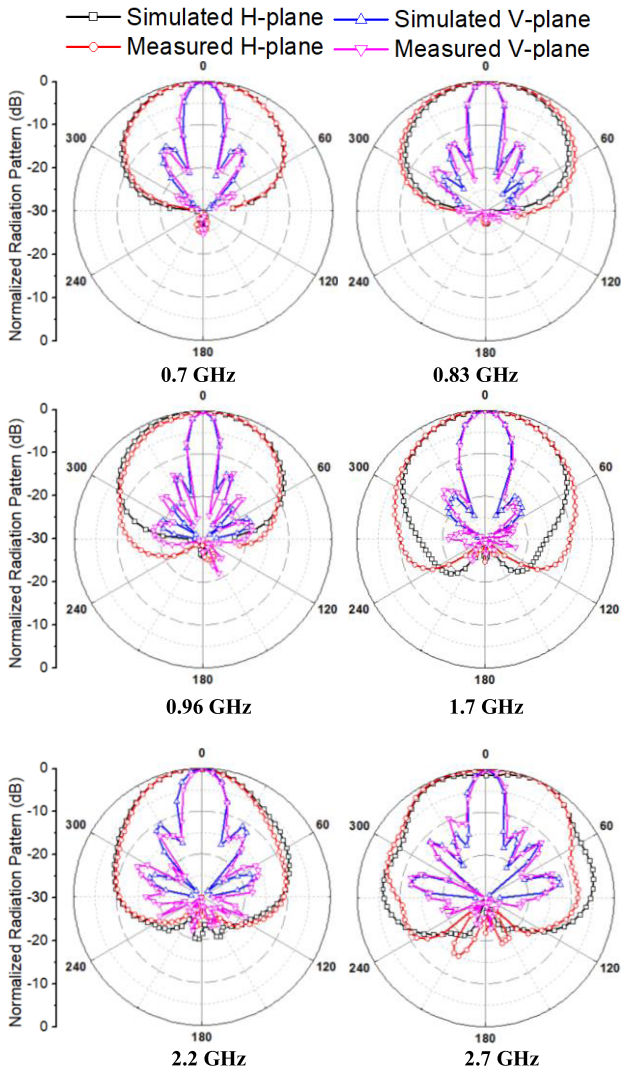

FIGURE 20. Simulated and measured radiation patterns of the prototype MIMO OLAS base station.

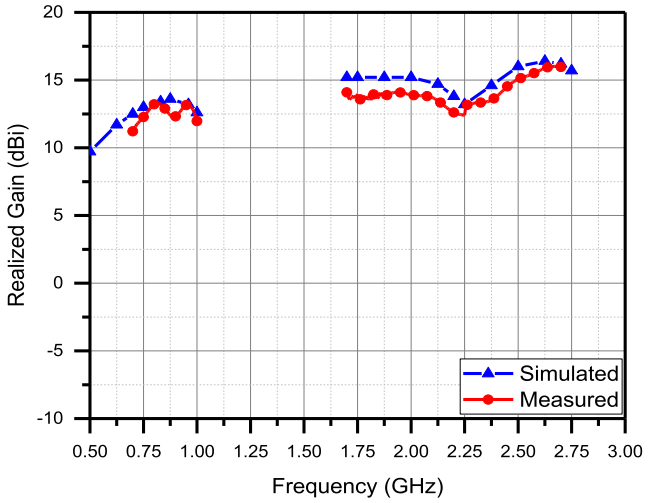

FIGURE 21. Simulated and measured realized gains of the prototype MIMO OLAS base station.

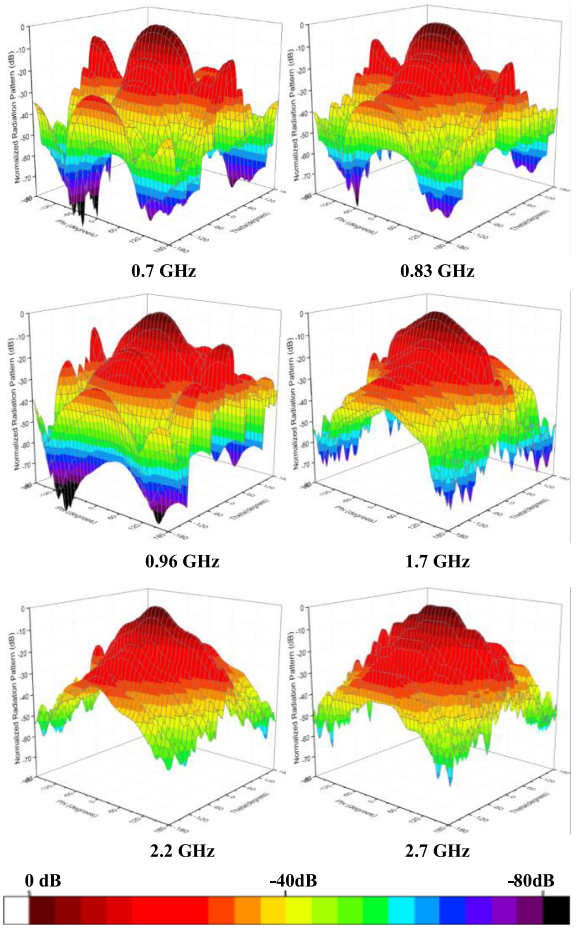

FIGURE 22. Normalized measured 3D radiation patterns of the prototype MIMO OLAS base station.

number of elements is eight elements while actually, the array consists of six elements as shown in Fig. 17. Again, the actual number of elements is less than the virtual number by 25%. The UB subarray consists of the middle elements numbering from 2 to 5 while the LB subarray consists of element numbered 1, 2, 5 and 6. Thus, element number 2 and 5 are shared elements.

To evaluate the diversity performance of the proposed MIMO system, the ECC should be obtained which is calculated for the four feeding ports P1, P2, P3 and P4 across the dual-band. ECC can be obtained as

$$ECC = \frac{\left|S_{ii}^{*}S_{ij} + S_{ji}^{*}S_{jj}\right|^{2}}{(1 - |S_{ii}|^{2} - \left|S_{ji}\right|^{2})(1 - \left|S_{jj}\right|^{2} - \left|S_{ij}\right|^{2})} \quad (2)$$

where each of i and j represents one of the feeding ports P1, P2, P3 or P4 and $i \neq j$. the polarization diversity is represented as the ECC of P1-P2 and P3-P4 while the frequency diversity is represented as the ECC of P1-P3 and P2-P4.

It worth noting that each pair of these ECC is reciprocal because of the array symmetrical feeding structure. The calculated ECC based on the measurements are plotted in Fig. 18. For simplicity, only the ECC of P1-P2,

TABLE 5. Measured parameters of the prototype MIMO OLAS base station.

Frequency Band	LB	UB
V-plane HPBW (°)	18±1	17±3
Realized Gain (dBi)	12.6±1.4	14±1.6
Front-to-Back lobe ratio (dB)	27	29

P1-P3 and P1-P4 are plotted. Results show that the proposed MIMO OLAS offer very low ECC due to the polarization and frequency diversities. The maximum ECC is less than 0.008 across the LB and less than 0.001 across the UB, far less than the general criteria of ECC < 0.3 [24].

The isolation between the dipoles of two adjacent elements (we take elements numbers 2 and 3 in Fig. 17 as an example) is measured and presented in Fig. 19. The isolation between the two orthogonal dipoles (dipoles 1 and 2) is similar to the isolation measured and presented in Fig. 7 for a single antenna element. For dipoles 1 and 3, the isolation at the LB is less than the isolation at the UB because the bowtie dipoles (which contribute in forming the LB radiation) are parallel and close to each other. That causes an electric field coupling between these two dipoles. Anyway, the worst case of isolation at the LB is close to 20 dB but it is better than 30 dB throughout the UB. For dipoles 1 and 4, isolation is better than 30 dB for both bands.

The prototype array radiation patterns and gains are measured using a VNA and an anechoic chamber. A good agreement between the simulated and the measured radiation patterns can be noticed in Fig. 20. The simulated and measured realized gains across both bands are presented in Fig. 21. The array measured parameters can be concluded in table 5. The normalized 3D measured radiation patterns for the prototype MIMO OLAS base station at the two bands are shown in Fig. 22 which demonstrate that both subarrays have stable radiation patterns across the bands of interest.

IV. CONCLUSION

A novel dual-broadband dual-polarized Fylfot-shaped antenna has been designed, optimized, fabricated and tested to cover two different bands 0.7 - 0.96 GHz and 1.7 - 2.7 GHz simultaneously for mobile communication systems. The proposed antenna has a high PP with a good impedance matching performance for both bands. In comparison to reference designs, the proposed design is much simpler as it uses a single element to cover both bands instead of two elements for two bands. In addition, the proposed antenna uses PCB manufacturing technology, which is easier than 3D printing used in reference designs.

A novel MIMO OLAS technique has been applied to form a dual-band linear array base station antenna with similar electrical performance as a conventional base station antenna but with 25% fewer number of elements and a remarkable smaller size, which makes the proposed design a good candidate for a low-cost directive base station antenna.

REFERENCES

[1] K. L. Wong, *Compact and Broadband Microstrip Antennas*. Hoboken, NJ, USA: Wiley, 2002, p. 10.
[2] X. P. Mao and J. W. Mark, "On polarization diversity in mobile communications," in *Proc. Int. Conf. Commun. Technol.*, Guilin, China, 2006, pp. 1–4.
[3] Q.-X. Chu, Y. Luo, and D.-L. Wen, "Three principles of designing base-station antennas," in *Proc. Int. Symp. Antennas Propag. (ISAP)*, Hobart, TAS, Australia, 2015, pp. 1–3.
[4] Y. Luo, Q.-X. Chu, and D.-L. Wen, "A plus/minus 45 degree dual-polarized base-station antenna with enhanced cross-polarization discrimination via addition of four parasitic elements placed in a square contour," *IEEE Trans. Antennas Propag.*, vol. 64, no. 4, pp. 1514–1519, Apr. 2016.
[5] A. S. Kaddour, S. Bories, A. Bellion, and C. Delaveaud, "3D printed compact dual-polarized wideband antenna," in *Proc. 11th Eur. Conf. Antennas Propag. (EUCAP)*, 2017, pp. 3452–3454.
[6] Y. He and W. Tian, "A broadband dual-polarized base station antenna element for European digital dividend, CDMA800 and GSM900 applications," in *Proc. 13th Int. Wireless Commun. Mobile Comput. Conf. (IWCMC)*, Valencia, Spain, 2017, pp. 659–663.
[7] Y. Cui, R. Li, and P. Wang, "Novel dual-broadband planar antenna and its array for 2G/3G/LTE base stations," *IEEE Trans. Antennas Propag.*, vol. 61, no. 3, pp. 1132–1139, Mar. 2013.
[8] X. Liu, S. He, H. Zhou, J. Xie, and H. Wang, "A novel low-profile, dual-band, dual-polarization broadband array antenna for 2G/3G base station," in *Proc. IET Int. Conf. Wireless, Mobile Multimedia Netw.*, Hangzhou, China, 2006, pp. 1–4.
[9] Y. He, Z. Pan, X. Cheng, Y. He, J. Qiao, and M. M. Tentzeris, "A novel dual-band, dual-polarized, miniaturized, and low-profile base station antenna," *IEEE Trans. Antennas Propag.*, vol. 63, no. 12, pp. 5399–5408, Dec. 2015.
[10] H. Huang, Y. Liu, and S. Gong, "A novel dual-broadband and dual-polarized antenna for 2G/3G/LTE base stations," *IEEE Trans. Antennas Propag.*, vol. 64, no. 9, pp. 4113–4118, Sep. 2016.
[11] G. Cui, S.-G. Zhou, G. Zhao, and S.-X. Gong, "A compact dual-band dual-polarized antenna for base station application," *Prog. Electromagn. Res. C*, vol. 64, pp. 61–70, 2016.
[12] Q. Chu, D. Zheng, and R. Wu, "Multi-array multi-band base-station antennas," in *Proc. Int. Workshop Antenna Technol., Small Antennas, Innov. Struct. Appl. (iWAT)*, Athens, Greece, 2017, pp. 137–139.
[13] Y.-B. Jung and S.-Y. Eom, "A compact multiband and dual-polarized mobile base-station antenna using optimal array structure," *Int. J. Antennas Propag.*, vol. 2015, 2015, Art. no. 178245.
[14] Y. He, W. Tian, and L. Zhang, "A novel dual-broadband dual-polarized electrical downtilt base station antenna for 2G/3G applications," *IEEE Access*, vol. 5, pp. 15241–15249, 2017.
[15] H. Huang, Y. Liu, and S. Gong, "A dual-broadband, dual-polarized base station antenna for 2G/3G/4G applications," *IEEE Antennas Wireless Propag. Lett.*, vol. 16, pp. 1111–1114, 2017.
[16] C. Beckman and B. Lindmark, "The evolution of base station antennas for mobile communications," in *Proc. Int. Conf. Electromagn. Adv. Appl.*, Turin, Italy, 2007, pp. 85–92.
[17] T.-W. Chiou and K.-L. Wong, "A compact dual-band dual-polarized patch antenna for 900/1800-MHz cellular systems," *IEEE Trans. Antennas Propag.*, vol. 51, no. 8, pp. 1936–1940, Aug. 2003.
[18] S. Nikmehr and K. Moradi, "Design and simulation of triple band GSM900/DCS1800/UMTS2100 MHz microstrip antenna for base station," in *Proc. IEEE Int. Conf. Commun. Syst.*, Singapore, Nov. 2010, pp. 113–116.
[19] P. Li, K. M. Luk, and K. L. Lau, "A dual-feed dual-band L-probe patch antenna," *IEEE Trans. Antennas Propag.*, vol. 53, no. 7, pp. 2321–2323, Jul. 2005.
[20] W. X. An, H. Wong, K. L. Lau, S. F. Li, and Q. Xue, "Design of broadband dual-band dipole for base station antenna," *IEEE Trans. Antennas Propag.*, vol. 60, no. 3, pp. 1592–1595, Mar. 2012.
[21] A. Alieldin and Y. Huang, "Design of broadband dual-polarized oval-shaped base station antennas for mobile systems," in *Proc. IEEE Int. Symp. Antennas Propag. USNC/URSI Nat. Radio Sci. Meeting*, San Diego, CA, USA, Jul. 2017, pp. 183–184.
[22] *Product Group: AltaFlex Tri-Sector*. Accessed: Jul. 1, 2018. [Online]. Available: https://alphaantennas.com/products/tri-sector/
[23] C. A. Balanis, *Antenna Theory Analysis, and Design*. Hoboken, NJ, USA: Wiley, 2005.
[24] H. Huang, X. Li, and Y. Liu, "5G MIMO antenna based on vector synthetic mechanism," *IEEE Antennas Wireless Propag. Lett.*, vol. 17, no. 6, pp. 1052–1055, Jun. 2018.

AHMED ALIELDIN received the B.Sc. degree in radar engineering from the Military Technical College, Egypt, in 2005, and the M.Sc. (Eng.) degree in antenna and microwave propagation from the University of Alexandria, Egypt, in 2013. He is currently pursuing the Ph.D. degree in electrical engineering with the University of Liverpool, U.K. He was a Radar Engineer with MoD, Egypt, and a Lecturer Assistant with the Air Defence College, Egypt. He was also an Antenna Engineer with Benha Electronics Company, where he was involved in the projects of national importance. His research interests include mobile base station antennas, satellite antennas, MIMO, and phased-MIMO radar antenna arrays design.

YI HUANG (S'91–M'96–SM'06) received the B.Sc. degree in physics and the M.Sc. (Eng.) degree in microwave engineering from Wuhan University, Wuhan, China, and the D.Phil. degree in communications from the University of Oxford, Oxford, U.K., in 1994.

He was with NRIET, Nanjing, China, as a Radar Engineer and in various periods with the Universities of Birmingham, U.K., Oxford, and Essex as a Research Staff Member. In 1994, he joined as a Research Fellow with British Telecom Labs, London, U.K., and then joined the Department of Electrical Engineering and Electronics, University of Liverpool, as a Lecturer, in 1995, where he is currently the Chair of wireless engineering, the Deputy Head of the department, the Head of the High-Frequency Engineering Research Group, and the M.Sc. Program Director. He has authored over 300 refereed papers in leading international journals and conference proceedings, and authored the books *Antennas: From Theory to Practice* (John Wiley, 2008) and *Reverberation Chambers* (Wiley, 2016). His current research interests include radio communications, applied electromagnetics, radars, and antennas.

He was a recipient of many research grants from research councils, government agencies, charity, EU, and industry, acted as a consultant to various companies, and served on a number of the national and international technical committees (such as the IET, EPSRC, European ACE, COST-IC0603, and COST-IC1102 and EurAAP). He has been an editor, an associate editor, or a guest editor of four of international journals. He has been a Keynote/Invited Speaker and an Organizer of many conferences and workshops (e.g., IEEE iWAT, WiCom, and LAPC). He is currently an Editor-in-Chief of *Wireless Engineering and Technology* (ISSN 2152-2294/2152-2308), an Associate Editor of the IEEE Antennas and Wireless Propagation Letters, a College Member of EPSRC, U.K./Ireland Delegate to EurAAP, and a fellow of the IEE/IET.

STEPHEN J. BOYES received the B.Eng. degree (Hons.) in electronic and communication engineering, the M.Sc. (Eng) degree in microelectronic systems and telecommunications, and the Ph.D. degree in antennas/electromagnetics from the University of Liverpool.

His academic research activities and Ph.D. at the University of Liverpool was centered on Reverberation Chambers, with an emphasis on a wide variety of antennas and antenna measurements for communication applications. His academic research work covered novel textile antennas, multiple-input multiple-output antennas, and novel antenna arrays.

In addition to work in academia, he has also held various positions throughout 10 years working in industry. In 2013, he joined the Defence Science and Technology Laboratory, where he is currently a Senior RF Research Scientist leading all antennas and electromagnetics research activities within his group. He holds numerous patents in the RF field. His present research interests and activities are associated with novel antennas for military applications, which include body worn and vehicle borne types. He also leads research into novel frequency selective surfaces, bespoke network configurations, and measurements with reverberation chambers.

He is the main author of a technical book on reverberation chambers published by John Wiley & Sons in 2016 and has also authored many papers in leading international journals and conferences. He serves as a technical reviewer for leading academic journals in the antennas and propagation field as well as sitting on major international committees on behalf of the U.K., chairing one such technical committee on novel antenna design.

MANOJ STANLEY received the B.Tech. degree in electronics and communication from Kerala University, India, in 2012, and the M.Tech. degree in communication systems from the Visvesvaraya National Institute of Technology, India, in 2014. He was a Lab Engineer with CoE, Visvesvaraya National Institute of Technology, where he was involved in the projects of national importance. He is currently pursuing the Ph.D. degree in electrical engineering with the University of Liverpool, U.K. His research interests include mobile phone antenna design, theory of characteristic modes, MIMO, and mm-wave antenna array design for 5G smartphones.

SUMIN DAVID JOSEPH received the B.Tech. degree (Hons.) in electronics and communication from the Cochin University of Science and Technology, India, in 2012, and the M.Tech. degree (Hons.) in communication systems from the Visvesvaraya National Institute of Technology, India, in 2015. He is currently pursuing the dual Ph.D. degrees in electrical engineering with the University of Liverpool, U.K., and National Tsing Hua University, Taiwan.

He was a Lab Engineer with CoE, Visvesvaraya National Institute of Technology, where he was involved in the projects of national importance. His research interests include self-biased circulators, mm-wave antenna arrays, rectifying antennas, rectifiers, wireless power transfer, and energy harvesting.

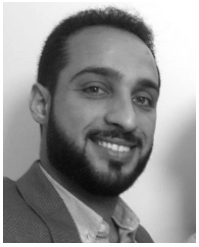

BAHAA AL-JUBOORI received the B.Sc. and M.Sc. degrees from the Department of Electronics and Communications Engineering, Al-Nahrain University, Baghdad, Iraq, in 2006 and 2010, respectively. He is currently pursuing the Ph.D. degree with the Department of Electrical Engineering and Electronics, University of Liverpool, Liverpool, U.K. He was a BSS Engineer with Motorola/Zain, Babylon, Iraq, from 2010 to 2012. Then, he was with Nokia Siemens Network as a Back Office Engineer until 2014. During that time, he was with EarthLink Telecommunications for Internet services as a part-time job. His current research interests include electromagnetic millimeter-wave filters, power dividers, couplers, and diplexers.